# Ground-State Geometry and Vibrations of Polyphenylenevinylene Oligomers

Nikita V. Tukachev,[†,‡] Dmitry R. Maslennikov,[‡,§] Andrey Yu. Sosorev,[‡,§] Sergei Tretiak,*[,†,∥] and Andriy Zhugayevych*[,†]

[†]Center for Energy Science and Technology, Skolkovo Institute of Science and Technology, Moscow 143026, Russia
[‡]Institute of Spectroscopy, Russian Academy of Sciences, Fizicheskaya 5, Troitsk, Moscow 108840, Russia
[§]Phaculty of Physics and International Laser Center, Lomonosov Moscow State University, Moscow 119991, Russia
[∥]Theoretical Division, Los Alamos National Laboratory, Los Alamos, New Mexico 87545, United States

**S** *Supporting Information*

**ABSTRACT:** Conformational space of polyphenylenevinylene oligomers is systematically investigated computationally at energies relevant for room temperature dynamics in a solvent and in a solid state. Our calculations show that optimal oligomer structures are essentially planar. However, lack of a deep minimum at the planar geometry allows for large molecular deformations even at very low temperatures. At larger angles, rotational motion of dihedrals intermix with two orthogonal bending motions of the entire molecule. In a crystalline environment these degrees of freedom intermix with translational and rotational motions, whereas purely intramolecular modes are well separated. The reliability of our calculations is confirmed by an excellent match of the theoretical and experimental Raman spectra of crystalline stilbene in the entire spectral range including the low-frequency part. Obtained results provide important insights into nature of low-frequency vibrations, which play a key role in charge transport in organic semiconductors.
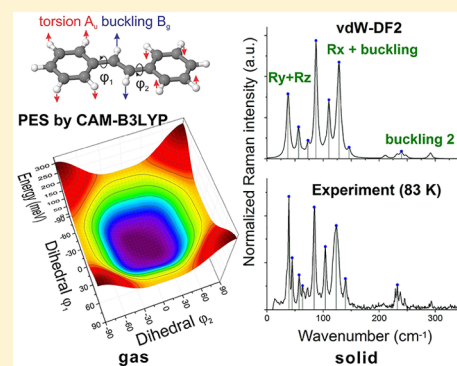
The poly(*p*-phenylenevinylene) (PPV) polymer and its oligomers (OPVs) are among the simplest and most thoroughly studied π-conjugated systems.[1−4] While electronic properties of the fully planar oligomers are well understood, description of nonplanarity effects is limited. The main challenge is the complex potential energy surface (PES) of this system with local minima and transition states at very low energies thermally accessible at room temperatures and below. While all nonrigid conjugated polymers and oligomers have large-amplitude modes (LAM) associated with rotation of flexible dihedrals, usually such rotations are dynamically independent. More challenging are systems with dynamically coupled LAMs, in the sense that considering dynamics of each dihedral separately is meaningless. An archetypal representative of this class is PPV having two coupled dihedrals per monomer (see Figure 1). In addition, the PES over these dihedrals is flat at millielectronvolt scale far away from the planar conformation. Because frontier electronic levels of π-conjugated molecules are highly sensitive to dihedrals, modulation of electronic properties due to electron-vibrational dynamics in PPV is highly nontrivial. Importantly, at the room temperature, activated low-frequency modes strongly scatter charge carriers and excitons imposing intrinsic limits on performance of optoelectronic devices.[5−9] Therefore, adequate description of LAMs and their interactions with intermolecular motions in solids is important for understanding and accurate description
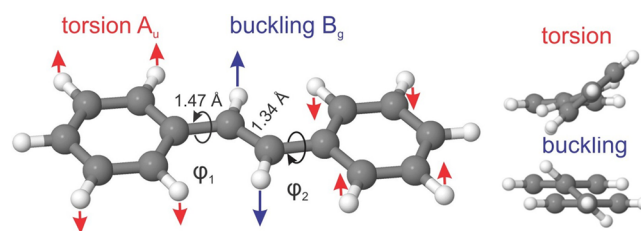


**Figure 1.** Geometric definitions for *trans*-stilbene (OPV2): the two interacting flexible dihedrals $\varphi_{1,2}$ and the corresponding collective LAMs, torsion and buckling.

of charge transport in organic semiconductors with nonrigid π-conjugated backbone.

In this work we focus on geometry and the low-energy region of the PES of PPV oligomers in both gas and solid states. Despite multiple experimental[10−12] and theoretical[13−18] investigations (see Section S2 of the Supporting Information), the gas-phase ground-state geometry remains uncertain even for the smallest oligomer, *trans*-stilbene (Figure 1), because small changes in total energy correspond to large changes in geometry. The key geometrical parameters of PPV oligomers
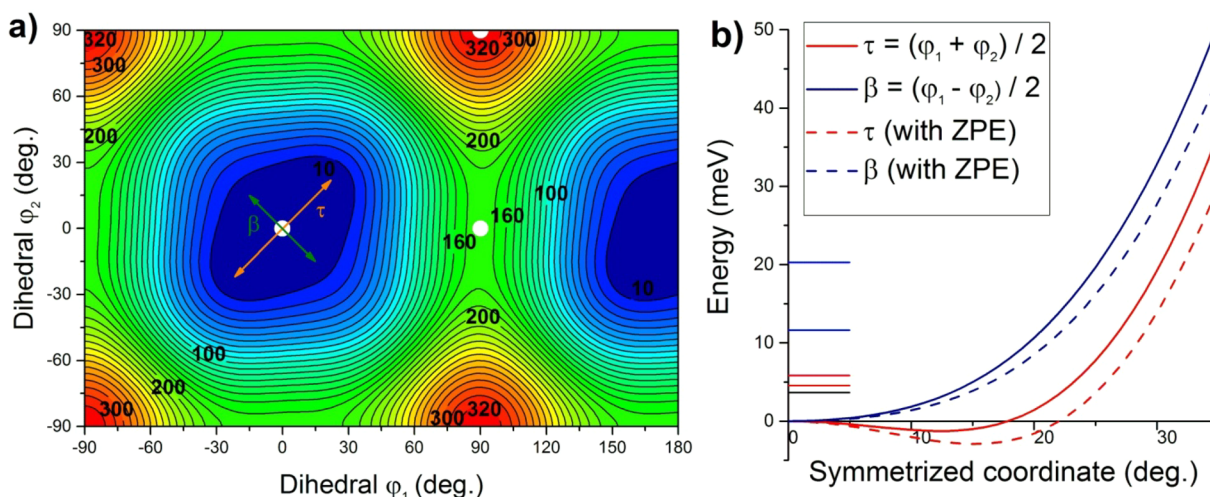
**Figure 2.** (a) Two-dimensional PES of *trans*-stilbene as computed by CAM-B3LYP/6-31G* with ZPE correction. Numeric labels on the contour lines correspond to energy in meV. Positions of the three stationary-by-symmetry points are shown as white dots (see also Table S1). Orange and green arrows show torsion ($\tau$) and buckling ($\beta$) mode directions. (b) PES cross sections along the symmetrized coordinates torsion $\tau$ and buckling $\beta$, together with the lowest energy levels of the two-dimensional quantum vibrational problem. (The zero-point level is marked by black line; torsion and buckling excitations are colored appropriately.) See more data in Figure S6.
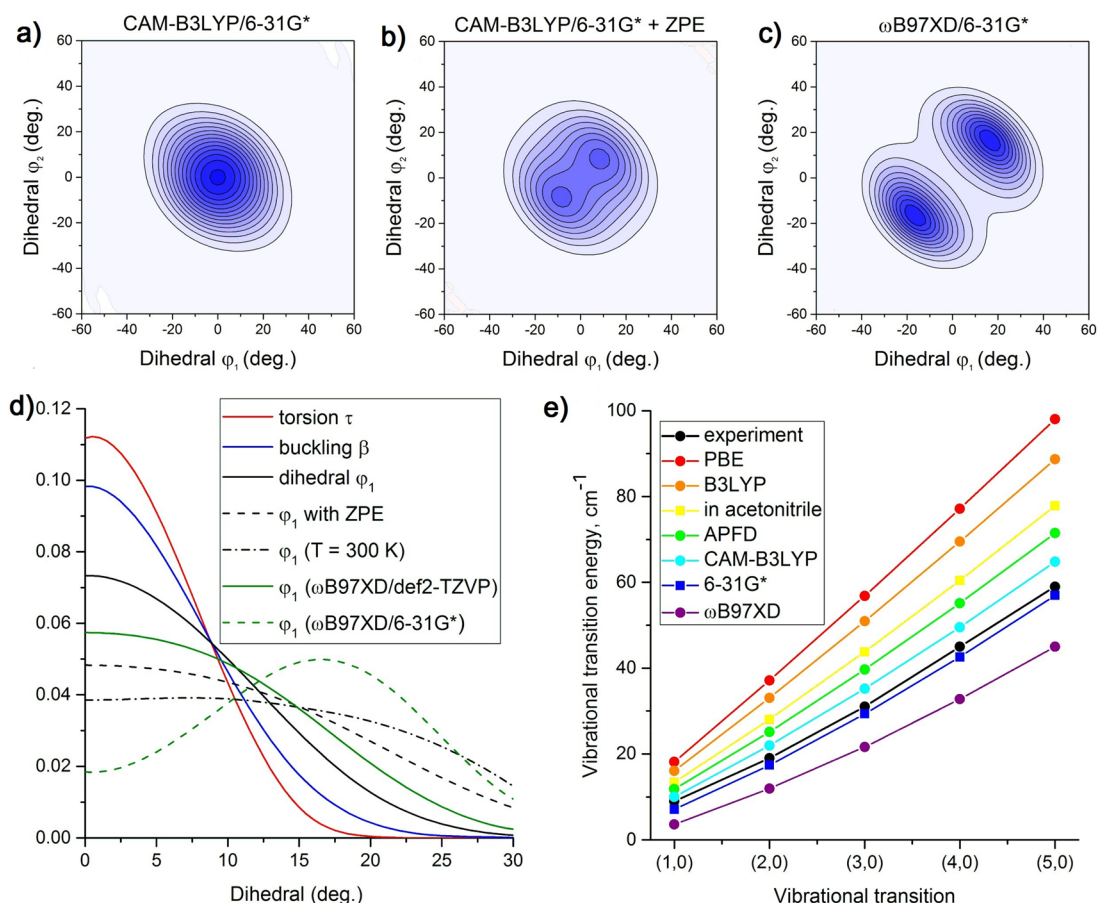


**Figure 3.** (a)−(c) Ground-state vibrational wave function of *trans*-stilbene. All considered methods give one of the three types of the ground state shown here: (a) single maximum, (b) two merging maxima, and (c) two well separated maxima. (See also Figure S10.) (d) Distribution of dihedral angles and their symmetric combinations for the ground-state vibrational wave function of *trans*-stilbene. The default method is CAM-B3LYP/6-31G*. (e) Vibrational transition energies calculated by different density functionals and compared to gas-phase experiment.[32] Here we use the def2-TZVP basis set except for "in acetonitrile", which means CAM-B3LYP/6-31G* calculations in the CPCM model of acetonitrile, and "6-31G*", which means our default method, CAM-B3LYP/6-31G*. Addition of ZPE correction uniformly decreases all energies, so that, e.g., CAM-B3LYP/def2-TZVP+ZPE data points are visually indistinguishable from CAM-B3LYP/6-31G* data. See more comparisons in Figure S5 and also torsion progression for styrene in Figure S7a.

are the bond length alternation (BLA) and the two flexible dihedrals $\varphi_{1,2}$ (per vinyl group) or their symmetric combinations: *torsion* $\tau = (\varphi_1 + \varphi_2)/2$ and *buckling* $\beta = (\varphi_1 - \varphi_2)/2$; see Figure 1 (also Tables S1 and S2). The experimental gas-phase geometry is published only for stilbene:[10] it was concluded that $\beta = 0$, $\tau \approx 30°$, whereas BLA could not be accurately determined. Experimentally resolved crystal structures[19−24] also do not provide a consistent value of BLA but converge on dihedrals: all oligomers and the polymer are reported to be flat without a systematic deviation from planarity. This is consistent with very small deplanarization energy gain (if any), so that intermolecular steric interactions easily planarize the molecules. Taking into account large uncertainty of experimental determination of BLA and dihedrals, vibrational spectroscopy becomes an important tool for indirectly probing the geometry of PPV oligomers using both empirical[25−27] and first-principles[13−16,28,29] models to match experimental spectra.[28−31] For the high-frequency region ($>400$ cm$^{-1}$), Raman spectra of PPV are well reproduced by harmonic approximation with scaled DFT frequencies. They are dominated by two strong Raman bands:[30,31] the band at 1600 cm$^{-1}$ corresponds to the BLA mode (alternating stretching of bonds), whereas the band at 1200 cm$^{-1}$ has a more complex nature. Modeling and interpretation of the low-frequency region ($<200$ cm$^{-1}$) is challenging due to effects of anharmonism (especially for LAMs) and mode mixing (especially for crystals). In particular, for the *trans*-stilbene molecule, there is no consensus on the exact shape of its low-energy PES and there are discrepancies in interpretation and first-principles simulation of observed vibrational spectra.[32−34] For low-frequency modes in crystals, experimental reports[35,36] provide only empirical interpretation of spectra using symmetry arguments and fitting oversimplified models, whereas first-principles simulations of Raman spectra have yet to be reported.

In summary, the analysis of literature suggests that even though PPV is a well-studied system, some fundamental questions concerning PES and, in particular, planarity of molecular geometry in the gas phase are left unanswered even for the shortest oligomer. The present work addresses these issues by answering questions: Which scalable method can accurately predict the PES? What is the ground-state geometry and what are low-energy conformers in vacuum? Which molecular motions contribute to low-frequency vibrational spectra in the gas phase and solid state? Our Letter is organized as follows: after benchmarking density functional theory (DFT) methods and choosing the most accurate one, we determine PES of stilbene molecule in a vacuum (Figure 2), calculate the vibrational wave function (Figure 3a−c), identify all low-frequency modes (Table 1), show agreement with experimental data on geometry (Figure 3d) and vibrations (Figure 3e), and then repeat this analysis for the crystal (Figure 4) and discuss other PPV oligomers.

Computational methodology is detailed in Section S3 of the Supporting Information. Briefly, we use Gaussian 16[37] and VASP[38] packages for calculations with Gaussian basis sets (up to quadruple-$\zeta$ quality) and with plane waves (600 eV cutoff, PAW pseudopotentials abbreviated as PAW600), respectively, as well as methods described in ref 39 for solution of vibrational problems. Most of the commonly used density functionals are thoroughly benchmarked in Section S4 of the Supporting Information and in refs 40 and 41. In addition, MP2 and CCSD(T) methods are applied for the stilbene

**Table 1. Calculated (CAM-B3LYP/6-31G\*) vs Experimental Frequencies (cm$^{-1}$) of *trans*-Stilbene in a Gas Phase$^a$**

| calc | exp | sym | physical interpretation |
|------|------|------|-------------------------|
| (7) | 8 | $A_u$ | torsion |
| (64) | | $B_g$ | buckling |
| 60 | 58 | $A_u$ | out-of-plane bending |
| 83 | 76 | $B_u$ | in-plane bending |
| 209 | 202 | $A_g$ | complex in-plane |
| 221 | $\approx 226$ | $B_g$ | buckling 2 |
| 291 | 291 | $A_g$ | in-plane bending 3 |
| 294 | $\approx 285$ | $A_u$ | out-of-plane bending 2 |

$^a$The values in parentheses are for the lowest transitions in the 2D vibrational problem, whereas the rest of frequencies are obtained in harmonic approximation for the planar conformation. Experimental data[32] contain five data sets; see Table S14 for details. The buckling mode is discussed in the text.

molecule. Judging by all available experimental and computed data on geometry and vibrations of PPV oligomers, the CAM-B3LYP/6-31G\* method provides a reasonable trade-off between the accuracy and computational cost. If accuracy is important, the def2-TZVP basis set gives results close to the complete basis set limit for DFT methods, though it is 2 times larger than 6-31G\*. Also, in terms of the accuracy of the stilbene PES, the $\omega$B97XD functional results seem to be closer to CCSD (basis set convergence has not been achieved) and MP2 predictions, whereas the CAM-B3LYP approach better matches observed vibrational frequencies. In any case, both functionals predict similar geometries and energies at def2-TZVP basis set. Among other tested functionals APFD predicts PES for dihedrals close to CAM-B3LYP but inaccurate BLA, and M06-2X gives PES close to $\omega$B97XD. The most sensitive parameter is the frequency of the buckling mode of the *trans*-stilbene: it varies from imaginary 10 meV for MP2 to real 10 meV for PBE. Consequently, most of the calculations in this work are performed using the CAM-B3LYP/6-31G\* method with D3 corrections[42] for intermolecular geometries. For plane waves, both considered functionals, PBE-D3 and vdW-DF2,[43,44] give reasonable accuracy for intermolecular geometry and vibrational frequencies in a crystal.

We start our investigation by analyzing geometry, PES, and vibrations of *trans*-stilbene molecule in vacuum. Important equilibrium geometry parameters and rotational constants of stilbene evaluated by different DFT methods are listed in Table S11. The entire PES over the two flexible dihedrals is shown in Figure 2, and almost all considered DFT functionals predict qualitatively the same picture: a minimum on PES corresponding to nonplanar conformation with nonzero torsion ($\tau \neq 0$, $\beta = 0$). The exceptions are PBE and B3LYP functionals predicting planar geometry, though for B3LYP some basis sets (e.g., TZVP) give slightly nonplanar geometry with planarization energy and dihedrals very close to 0. Functionals with high Hartree−Fock exchange fraction ($\omega$B97XD, LC-$\omega$PBE) and MP2 predict also the secondary minimum with nonzero buckling ($\tau = 0$, $\beta \neq 0$).

Because the PES is so flat, the molecular geometry at the PES minimum does not answer the question of whether or not *trans*-stilbene is planar in the ground electronic state, since the observable geometry can be different due to quantum and thermal fluctuations. To take into account quantum fluctuations, the wave function of the lowest vibrational levels is
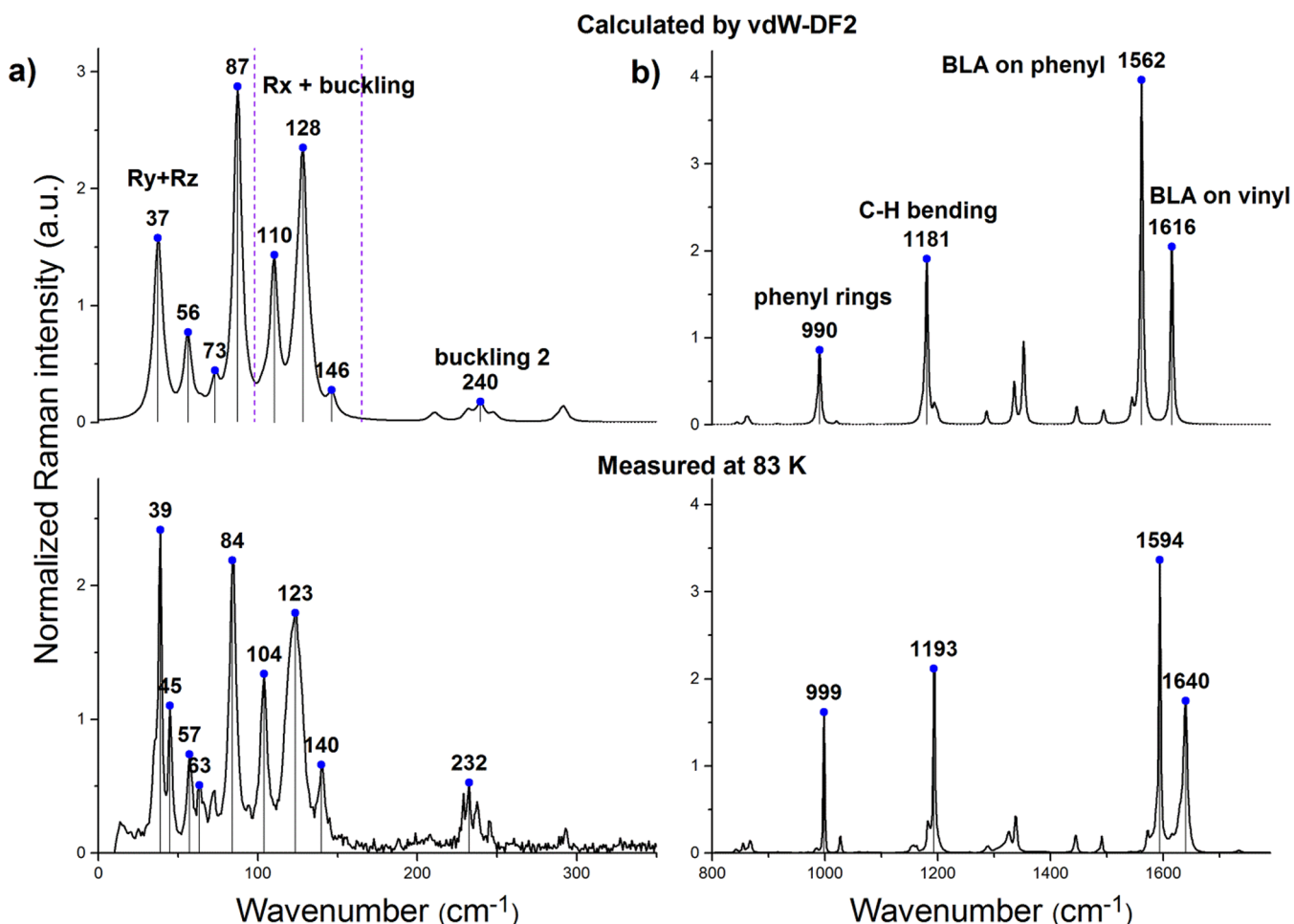
**Figure 4.** Calculated vs experimental Raman spectra of the stilbene crystal. Numbers at peaks denote maxima of the corresponding bands. "Rx +buckling" means intermixed long-axis rotation and buckling, "Ry+Rz" are short-axes rotations, and the dashed lines separate these two groups of vibrational modes. See Tables S14 and S16 for details.

calculated and shown in Figure 3a−c and Figure S10. As expected, for PES with deep minima at $\tau = \pm \tau_0$ (e.g., $\omega$B97XD/6-31G*) the lowest energy wave function has two clearly separated domains (Figure 3c), whereas for shallow minima (e.g., CAM-B3LYP, $\omega$B97XD/def2-TZVP) the wave function is delocalized among those minima (Figure 3a,b). In the latter case, the probability distribution function of angles, Figure 3d, shows no deep minimum (if any) at zero, implying that the observable geometry is planar. At the same time, the distribution is broad spanning up to 30° in good agreement with experiment,[10] especially at elevated temperatures due to the addition of thermal fluctuations. Since the above results are highly sensitive to computational method, we use experimentally probed energies of the lowest vibrational transitions[32] to benchmark the methodology. The comparison given in Figure 3e and Figure S5 shows that CAM-B3LYP best matches the experiment, and this was one of the tests used to select CAM-B3LYP as the default functional for this work. It should be noted that the MP2-based basis set extrapolation of CCSD sampling of the PES is more consistent with the $\omega$B97XD functional with a large enough basis set; see Figure S6c (and also the (1,0) transition can be missed in analysis of experimental spectra if its frequency is close to zero). However, as shown in Figures 3d and S10, both $\omega$B97XD with large basis set and CAM-B3LYP predict essentially the same double-well PES and wave function but single-humped dihedral angle

distribution. Also, ZPE corrections are of the same order as basis set corrections; e.g., predicted wave function (Figure S10e) and transition energies for CAM-B3LYP/def2-TZVP with ZPE are close to those for CAM-B3LYP/6-31G* without ZPE.

The rest of the low-frequency vibrations are summarized in Table 1, showing good agreement of calculations with experiment. The only difference from ref 32 is that the tiny peak in the fluorescence excitation spectrum at 118 cm$^{-1}$ was interpreted as the buckling mode frequency, whereas we assign it to an overtone or a combination of interacting lower frequency modes, since there are three of them near the half-frequency complicating interpretation of the observed spectra. In fact, the "in-plane bending" mode varies substantially on the two-dimensional PES and intermixes with the buckling mode (Figure S3). Quantitative estimates require solution of at least three-dimensional vibrational problem which is beyond the scope of this work.

In a solid state we expect a dramatic change of PES of intramolecular LAMs due to intermolecular interactions among which steric constraints are the most important parameters.[45] Moreover, molecular solids have an additional set of modes resembling LAMs of free molecules: intermolecular modes corresponding to translational and rotational motions of individual molecules, which are usually anharmonic and intermixed. The entire set of such low-frequency modes

presents a challenge for their description in contrast to phonons in rigid solids and vibrations in rigid molecules.

To study how PES of the two dihedrals changes in the crystalline environment, we select a molecule-centered cluster containing all essential contact interactions with the central molecule (12 neighbors). The cluster is cut out of the crystal fully relaxed by the PBE-D3/PAW600 method; then in the PES scan by CAM-B3LYP/6-31G* we allow only the central molecule to move (the robustness of the model with respect to implicit and explicit solvation effects has been tested in Table S15). The resulting PES shown in Figure S11 is drastically different from that in Figure 2a; namely, it is no longer flat. Moreover, even at relatively significant deviations from equilibrium (within 30° in $\tau$, $\beta$ and 100 meV in energy), the PES is essentially harmonic (Figure S12). Thus, counterintuitively, low-energy PES in a crystal is simpler than that in a free molecule.

Because PES in a crystal is nearly harmonic, the Hessian diagonalization at the minimum should give accurate vibrational spectra. To decompose phonons into motions of individual molecules we use perturbation analysis of the Γ-point force constant matrix calculated by the PBE-D3/PAW600 method following our previous work[46] (see details in the Supporting Information, p S9). The lowest 12 modes per molecule (discussed below) are given in Table S15. In a crystalline environment, stilbene is a relatively rigid molecule with the smallest vibrational frequency at 5 meV, whereas the torsion and buckling frequencies are increased to about 15 meV. Since PES is no longer flat, different density functionals give consistent results, in a sharp contrast with the Hessian of the free molecule. Vibrational modes above 25 meV (200 cm$^{-1}$) are intramolecular: they do not intermix with other modes and their dispersion is negligible (~1 meV). Low-frequency modes (10 modes per molecule) intermix and have noticeable dispersion with 5−14 meV bandwidth. The only exception is the torsion mode preserving intramolecular character despite the resonance with other modes (in a crystal its frequency is increased substantially), which is probably due to unique symmetry of this mode. Thus, we see that mode mixing and change of PES substantially modify character and frequencies of the lowest normal modes in a crystal compared to a free molecule, complicating their cross-identification solely by vibrational spectra:[36] even the mode ordering changes so that the torsional progression that is well-separated in the gas-phase moves up in energy in the crystal slightly above the buckling mode energy.

To check the reliability of our crystal modeling, we have measured and simulated Raman spectrum of crystalline stilbene; see details in Section S10 of the Supporting Information. The results are compared in Figure 4 showing an excellent agreement between experiment and theory at the vdW-DF2 level. Our calculations show that all Raman-active modes below 200 cm$^{-1}$ belong to two groups: the group below 100 cm$^{-1}$ is assigned to molecular rotations $R_y$ and $R_z$ (short axes), whereas the other peaks correspond to the intermixed long-axis rotation $R_x$ and buckling. This is consistent with symmetry analysis forbidding odd modes ($A_u$ and $B_u$; see Table S14) in the dipole approximation.

Finally, we briefly discuss geometry of longer oligomers. Distyrylbenzene (OPV3) is the next smallest PPV oligomer suitable to study effects of weak interactions between strongly coupled pairs of dihedrals, which are separated by the middle phenyl ring. There are four possible low-energy conformers

distinguished by the sequence of the signs of the four flexible dihedrals;[47] see Table S2. In agreement with previous studies,[47] the lowest energy conformer (for all considered methods) corresponds to the helical torsion, where all signs are equal $(++++)$. The next conformer corresponds to the alternating torsion $(++--)$. Here the energy difference is only 0.5 meV, giving the minor penalty of changing sign of dihedrals across the middle phenyl ring. The other two conformations would represent helical and alternating buckling, but it turns out that buckling is energetically suppressed in OPV3 and longer oligomers. Consequently, all low-energy conformers of any oligomer OPVn can be represented as sequences of torsions, and the total energy relative to the planar conformation can be estimated as $E_n = (n - 1)E_{torsion} + (n - 2)E_{coupling} + mE_{defect}$, where $E_{torsion}$ is a torsion energy per vinyl group (−1.4 meV for CAM-B3LYP/6-31G*), $E_{coupling}$ is an across-ring coupling energy (+1.0 meV), $m$ is the number of sign changes ("defects"), and $E_{defect}$ is the defect creation penalty (+0.5 meV); see Table S17. Since $E_{coupling}$ is positive due to $\pi$-conjugation, the tendency to planarization strengthens with oligomer size: the planarization energy gain decreases from 1.4 meV for stilbene to 0.4 meV for the polymer (and the same trend holds for imaginary frequencies at the planar geometry; see Table S18).

Extensive DFT benchmarking made in this work allows us also to draw important conclusions on the use of density functionals for $\pi$-conjugated molecules. First of all, it should be noted that for any DFT modeling of complex systems, a good agreement with experimental measurements can be interpreted as the effect of some underlying error cancellation.[48] Consequently, a rigorous benchmarking per studied system is normally required to understand the performance of DFT models as illustrated in the present Letter for PPV oligomers. However, many density functionals show good transferability and very systematic trends,[49] and our data fully support this idea as well. In particular, benchmarks of torsional progression for stilbene and styrene molecules show essentially the same performance of the tested DFT models with respect to experimental and MP2/CCSD values (Table S8, Figure S7). Also, predictions of the studied transferable functionals PBE, B3LYP, PBE0, CAM-B3LYP, and $\omega$B97X are strictly ordered (systematic) in the sense that, e.g., the values of intramolecular properties (BLA, dihedrals, PES extrema, vibrational transition energies etc.) calculated by CAM-B3LYP are between PBE0 and $\omega$B97X values (deviations from this rule are much smaller than absolute errors of these functionals); see Tables S5a, S6a, S8, and S18. Moreover, the accuracy of these functionals strongly correlates with the "IP+EHOMO" descriptor[40] (see Figure S4), which is the sum of the ionization potential and the energy of the highest occupied molecular orbital (it is zero in ideal DFT[50]), thus supporting the idea that it can be used for assessment of density functionals for longer oligomers when experimental or high-level theory reference data are not available.

To summarize, via proper choice of the computational methodology, we have resolved the long-standing problem of the ground-state geometry of PPV oligomers. Although the PES of PPV oligomers has a shallow global minimum corresponding to the helical torsion of the oligomer, the ground-state vibrational wave function is delocalized between the two symmetry-equivalent minima. Consequently, the geometry is effectively planar at ambient and lower temperatures, though the distribution of the observable value of the

dihedrals is very broad (up to 30° for *trans*-stilbene) even at zero temperature. At the room temperature the molecule is also statistically planar, however, with even broader dihedral angle distribution. Due to extended $\pi$-conjugation, planarity improves with an increase of the oligomer size since both torsion angle and planarization energy per monomer decrease.

In a crystal, PESs of individual molecules become close to harmonic, so that, counterintuitively, description of vibrations in the crystal is simpler and less method-sensitive compared to the free molecule, which is also confirmed by a good agreement between measured and simulated Raman spectra in the entire range of vibrational frequencies. Mode analysis of stilbene crystal shows a clear separation of low-frequency modes: all vibrations above 200 cm$^{-1}$ are intramolecular meaning that they are linear combinations of undistorted normal modes of the free molecule. In contrast, there are 10 low-frequency modes per molecule (including translations and rotations) that strongly intermix and are dispersive in a crystal. Four of them are Raman-active being rotational and buckling motions.

From the perspective of charge transport in crystalline organic semiconductors, such a rich spectrum of low-frequency modes results in quasistatic and dynamic disorders at ambient conditions, which effectively decrease charge carrier transport via various scattering mechanisms. For example, such motions in OPV crystals produce large disorder, disrupting formation of ideal two-dimensional dispersive bands (Figure S14). Indeed, while molecular size, number of rotatable dihedrals, planarity, and even intermolecular electronic couplings (Table S20) in stilbene match those of TCNQ, practically achievable charge carrier mobility ($\mu$) differs substantially: TCNQ-core molecular crystals demonstrate good charge transport performance ($\mu \geq 1$ cm$^2$/(V s)) across the family,[51,52] whereas there are no published reports on high charge carrier mobility in OPV-core crystals ($\mu \leq 0.1$ cm$^2$/(V s)) in the sense of rigorously measured mobility in a field effect transistor.[4,24,53] A notable difference between these two molecules is that the two rotatable dihedrals of TCNQ are more rigid then those of stilbene, so that both thermal (due to low-frequency modes) and frozen-in (due to large amplitude motions) disorder would be lower in TCNQ crystals. At the same time, a reinforcement of the OPV core by modification of the vinyl bridge increases the mobility.[54−56] In this context, our study facilitates further research on understanding and controlling the relationships between low-frequency vibrational motions and charge transport efficiency in organic semiconductors.

## ASSOCIATED CONTENT

**Ⓢ Supporting Information**

The Supporting Information is available free of charge on the ACS Publications website at DOI: 10.1021/acs.jpclett.9b01200.

> Literature review, geometric definitions, computational and experimental details, benchmarks, geometry and rotational constants, PES, vibrational and Raman spectra, data for longer oligomers, and electronic couplings and band structure (PDF)

## AUTHOR INFORMATION

**Corresponding Authors**

*E-mail: serg@lanl.gov (S.T.).

*E-mail: a.zhugayevych@skoltech.ru (A.Z.).

**ORCID** ⊙

Nikita V. Tukachev: 0000-0002-2647-447X

Andrey Yu. Sosorev: 0000-0001-9343-5502

Sergei Tretiak: 0000-0001-5547-3647

Andriy Zhugayevych: 0000-0003-4713-1289

**Notes**

The authors declare no competing financial interest.

## ACKNOWLEDGMENTS

## REFERENCES

(1) Fink, J. K., Poly(arylene vinylene)s. *High Performance Polymers*; Plastics Design Library, 2008; pp 89−137.

(2) Blom, P. W. M.; Vissenberg, M. C. J. M. Charge transport in poly(p-phenylene vinylene) light-emitting diodes. *Mater. Sci. Eng., R* **2000**, *27*, 53−94.

(3) Ostroverkhova, O. Organic Optoelectronic Materials: Mechanisms and Applications. *Chem. Rev.* **2016**, *116*, 13279−13412.

(4) Wang, C.; Dong, H.; Jiang, L.; Hu, W. Organic semiconductor crystals. *Chem. Soc. Rev.* **2018**, *47*, 422−500.

(5) Zhugayevych, A.; Tretiak, S. Theoretical Description of Structural and Electronic Properties of Organic Photovoltaic Materials. *Annu. Rev. Phys. Chem.* **2015**, *66*, 305−330.

(6) Illig, S.; Eggeman, A. S.; Troisi, A.; Jiang, L.; Warwick, C.; Nikolka, M.; Schweicher, G.; Yeates, S. G.; Geerts, Y. H.; Anthony, J. E.; Sirringhaus, H. Reducing dynamic disorder in small-molecule organic semiconductors by suppressing large-amplitude thermal motions. *Nat. Commun.* **2016**, *7* (1−10), 10736.

(7) Fratini, S.; Mayou, D.; Ciuchi, S. The Transient Localization Scenario for Charge Transport in Crystalline Organic Materials. *Adv. Funct. Mater.* **2016**, *26*, 2292−2315.

(8) Chernyshov, I.Yu.; Vener, M. V.; Feldman, E. V.; Paraschuk, D.Yu.; Sosorev, A.Yu. Inhibiting Low-Frequency Vibrations Explains Exceptionally High Electron Mobility in 2,5-Difluoro-7,7,8,8-tetracyanoquinodimethane (F2-TCNQ) Single Crystals. *J. Phys. Chem. Lett.* **2017**, *8*, 2875−2880.

(9) Sosorev, A.Yu.; Maslennikov, D. R.; Kharlanov, O. G.; Chernyshov, I.Yu.; Bruevich, V. V.; Paraschuk, D.Yu. Impact of Low-Frequency Vibrations on Charge Transport in High-Mobility Organic Semiconductors. *Phys. Status Solidi RRL* **2018**, *13* (1−23), 1800485.

(10) Traetteberg, M.; Frantsen, E. B.; Mijlhoff, F. C.; Hoekstra, A. A Gas Electron Diffraction Study of the Molecular Structure of trans-Stilbene. *J. Mol. Struct.* **1975**, *26*, 57−68.

(11) Champagne, B. B.; Pfanstiel, J. F.; Plusquellic, D. F.; Pratt, D. W.; van Herpen, W. M.; Meerts, W. L. trans-Stilbene. A rigid, planar asymmetric top in the zero-point vibrational levels of its S$_0$ and S$_1$ electronic states. *J. Phys. Chem.* **1990**, *94*, 6−8.

(12) Woo, H. S.; Lhost, O.; Graham, S. C.; Bradley, D. D. C.; Friend, R. H.; Quattrocchi, C.; Brédas, J. L.; Schenk, R.; Müllen, K. Optical spectra and excitations in phenylene vinylene oligomers. *Synth. Met.* **1993**, *59*, 13−28.

(13) Watanabe, H.; Okamoto, Y.; Furuya, K.; Sakamoto, A.; Tasumi, M. Vibrational Analysis of trans-Stilbene in the Ground and Excited Singlet Electronic States Revisited. *J. Phys. Chem. A* **2002**, *106*, 3318−3324.

(14) Choi, C. H.; Kertesz, M. Conformational Information from Vibrational Spectra of Styrene, trans-Stilbene, and cis-Stilbene. *J. Phys. Chem. A* **1997**, *101*, 3823−2831.

(15) Baker, J.; Wolinski, K. Isomerization of Stilbene Using Enforced Geometry Optimization. *J. Comput. Chem.* **2011**, *32*, 43−53.

(16) Chen, P. C.; Chieh, Y. C. Azobenzene and Stilbene: A Computational Study. *J. Mol. Struct.: THEOCHEM* **2003**, *624*, 191−200.

(17) Kwasniewski, S. P.; Claes, L.; François, J.-P.; Deleuze, M. S. High level theoretical study of the structure and rotational barriers of trans-stilbene. *J. Chem. Phys.* **2003**, *118*, 7823−7836.

(18) Panda, A. N.; Plasser, F.; Aquino, A. J. A.; Burghardt, I.; Lischka, H. Electronically Excited States in Poly(p-phenylenevinylene): Vertical Excitations and Torsional Potentials from High-Level Ab Initio Calculations. *J. Phys. Chem. A* **2013**, *117*, 2181−2189.

(19) Varghese, S.; Park, S. K.; Casado, S.; Fischer, R. C.; Resel, R.; Milián-Medina, B.; Wannemacher, R.; Park, S. Y.; Gierschner, J. Stimulated Emission Properties of Sterically Modified Distyrylbenzene-Based H-Aggregate Single Crystals. *J. Phys. Chem. Lett.* **2013**, *4*, 1597−1602.

(20) van Hutten, P. F.; Wildeman, J.; Meetsma, A.; Hadziioannou, G. Molecular Packing in Unsubstituted Semiconducting Phenylenevinylene Oligomer and Polymer. *J. Am. Chem. Soc.* **1999**, *121*, 5910−5918.

(21) Granier, T.; Thomas, E. L.; Gagnon, D. R.; Karasz, F. E.; Lenz, R. W. Structure Investigation of Poly(p-Phenylene Vinylene). *J. Polym. Sci., Part B: Polym. Phys.* **1986**, *24*, 2793−2804.

(22) Mao, G.; Fischer, J. E.; Karasz, F. E.; Winokur, M. J. Nonplanarity and ring torsion in poly(p-phenylene vinylene). A neutron-diffraction study. *J. Chem. Phys.* **1993**, *98*, 712−716.

(23) Harada, J.; Ogawa, K. X-ray diffraction analysis of non-equilibrium states in crystals: observation of an unstable conformer in flash-cooled crystals. *J. Am. Chem. Soc.* **2004**, *126*, 3539−3544.

(24) Kabe, R.; Nakanotani, H.; Sakanoue, T.; Yahiro, M.; Adachi, C. Effect of Molecular Morphology on Amplified Spontaneous Emission of Bis-Styrylbenzene Derivatives. *Adv. Mater.* **2009**, *21*, 4034−4038.

(25) Tian, B.; Zerbi, G.; Schenk, R.; Müllen, K. Optical spectra and structure of oligomeric models of polyparaphenylenevinylene. *J. Chem. Phys.* **1991**, *95*, 3191−3197.

(26) Hernandez, V.; Castiglioni, C.; Del Zoppo, M.; Zerbi, G. Confinement potential and n-electron delocalization in polyconjngated organic materials. *Phys. Rev. B: Condens. Matter Mater. Phys.* **1994**, *50*, 9815−9823.

(27) Haller, K.; Chiang, W.- Y.; del Rosario, A.; Laane, J. High-Temperature Vapor-Phase Raman Spectra and Assignment of The Low-Frequency Modes of trans-Stilbene and 4-Methoxy-trans-stilbene. *J. Mol. Struct.* **1996**, *379*, 19−23.

(28) Egawa, T.; Shinashi, K.; Ueda, T.; Ocola, E. J.; Chiang, W.-Y.; Laane, J. Vapor-Phase Raman Spectra, Theoretical Calculations and the Vibrational and Structural Properties of cis- and trans-Stilbene. *J. Phys. Chem. A* **2014**, *118*, 1103−1112.

(29) Massuyeau, F.; Faulques, E.; Latouche, C.; Barone, V. New insights into the vibrational and optical signatures of trans-stilbene via integrated experimental and quantum mechanical approaches. *Phys. Chem. Chem. Phys.* **2016**, *18*, 19378−19385.

(30) Gierschner, J.; Mack, H.-G.; Lüer, L.; Oelkrug, D. Fluorescence and absorption spectra of oligophenylenevinylenes: Vibronic coupling, band shapes, and solvatochromism. *J. Chem. Phys.* **2002**, *116*, 8596−8609.

(31) Nguyen, T. P.; Yang, S. H.; Gomes, J.; Wong, M. S. Optical properties of nanosize aggregation of phenylene vinylene oligomers. *Synth. Met.* **2005**, *151*, 269−274.

(32) Chiang, W.-Y.; Laane, J. Fluorescence Spectra and Torsional Potential Functions for trans-Stilbene in its $S_0$ and $S_1(\pi,\pi)$ Electronic States. *J. Chem. Phys.* **1994**, *100*, 8755−8767.

(33) Orlandi, G.; Gagliardi, L.; Melandri, S.; Caminati, W. Torsional Potential Energy Surfaces and Vibrational Levels in trans-Stilbene. *J. Mol. Struct.* **2002**, *612*, 383−391.

(34) Chowdary, P. D.; Martinez, T. J.; Gruebele, M. The vibrationally adiabatic torsional potential energy surface of trans-stilbene. *Chem. Phys. Lett.* **2007**, *440*, 7−11.

(35) Papanek, P.; Fischer, J. E.; Sauvajol, J. L.; Dianoux, A. J.; Mao, G.; Winokur, M. J.; Karasz, F. E. Inelastic-neutron-scattering studies of poly(p-phenylene vinylene). *Phys. Rev. B: Condens. Matter Mater. Phys.* **1994**, *50*, 15668−15677.

(36) Bree, A.; Edelson, M. An investigation of the low-frequency torsional modes of trans-stilbene using Raman spectroscopy. *Chem. Phys.* **1980**, *51*, 77−88.

(37) Frisch, M. J.; Trucks, G. W.; Schlegel, H. B.; Scuseria, G. E.; Robb, M. A.; Cheeseman, J. R.; Scalmani, G.; Barone, V.; Mennucci, B.; Petersson, G. A.; et al. *Gaussian 09*, Revision A.02; Gaussian, Inc.: Wallingford, CT, 2009.

(38) Kresse, G.; Furthmüller, J. Efficient iterative schemes for ab initio total-energy calculations using a plane-wave basis set. *Phys. Rev. B: Condens. Matter Mater. Phys.* **1996**, *54*, 11169−11186.

(39) Tukachev, N. V.; Bataev, V. A.; Abramenkov, A. V.; Godunov, I. A. Structure and conformational dynamics of a formamide molecule in the ground and lowest excited electronic states. *Comput. Theor. Chem.* **2016**, *1080*, 23−32.

(40) Zhugayevych, A.; Postupna, O.; Wang, H. L.; Tretiak, S. Modification of optoelectronic properties of conjugated oligomers due to donor/acceptor functionalization: DFT study. *Chem. Phys.* **2016**, *481*, 133−143.

(41) Zhugayevych, A.; Mazaleva, O.; Naumov, A.; Tretiak, S. Lowest-Energy Crystalline Polymorphs of P3HT. *J. Phys. Chem. C* **2018**, *122*, 9141−9151.

(42) Grimme, S.; Ehrlich, S.; Goerigk, L. Effect of the damping function in dispersion corrected density functional theory. *J. Comput. Chem.* **2011**, *32*, 1456−1465.

(43) Klimes, J.; Bowler, D. R.; Michaelides, A. Van der Waals density functionals applied to solids. *Phys. Rev. B: Condens. Matter Mater. Phys.* **2011**, *83*, 195131−13.

(44) Brown-Altvater, F.; Rangel, T.; Neaton, J. B. Ab initio phonon dispersion in crystalline naphthalene using van der Waals density functionals. *Phys. Rev. B: Condens. Matter Mater. Phys.* **2016**, *93* (1−8), 195206.

(45) Goetz, K. P.; Fonari, A.; Vermeulen, D.; Hu, P.; Jiang, H.; Diemer, P. J.; Ward, J. W.; Payne, M. E.; Day, C. S.; Kloc, C.; Coropceanu, V.; McNeil, L. E.; Jurchescu, O. D. Freezing-in orientational disorder induces crossover from thermally-activated to temperature-independent transport in organic semiconductors. *Nat. Commun.* **2014**, *5* (1−8), 5642.

(46) Belyanchikov, M. A.; Zhukova, E. S.; Tretiak, S.; Zhugayevych, A.; Dressel, M.; Uhlig, F.; Smiatek, J.; Fyta, M.; Thomas, V. G.; Gorshunov, B. P. Vibrational states of nano-confined water molecules in beryl investigated by first-principles calculations and optical experiments. *Phys. Chem. Chem. Phys.* **2017**, *19*, 30740−30748.

(47) Lagowski, J. B. Ab initio investigation of conformational and excitation energies of phenylene vinylene oligomers. *J. Mol. Struct.: THEOCHEM* **2002**, *589−590*, 125−137.

(48) Medvedev, M. G.; Bushmarinov, I. S.; Sun, J.; Perdew, J. P.; Lyssenko, K. A. Density functional theory is straying from the path toward the exact functional. *Science* **2017**, *355*, 49.

(49) Sutton, C.; Sears, J. S.; Coropceanu, V.; Bredas, J. L. Understanding the density functional dependence of DFT-calculated electronic couplings in organic semiconductors. *J. Phys. Chem. Lett.* **2013**, *4*, 919−924.

(50) Autschbach, J.; Srebro, M. Delocalization Error and "Functional Tuning" in Kohn-Sham Calculations of Molecular Properties. *Acc. Chem. Res.* **2014**, *47*, 2592−2602.

(51) Menard, E.; Podzorov, V.; Hur, S.; Gaur, A.; Gershenson, M.; Rogers, J. High-Performance n- and p-Type Single-Crystal Organic Transistors with Free-Space Gate Dielectrics. *Adv. Mater.* **2004**, *16*, 2097−2101.

(52) Krupskaya, Y.; Gibertini, M.; Marzari, N.; Morpurgo, A. F. Band-Like Electron Transport with Record-High Mobility in the TCNQ Family. *Adv. Mater.* **2015**, *27*, 2453.

(53) Choi, H. H.; Cho, K.; Frisbie, C. D.; Sirringhaus, H.; Podzorov, V. Critical assessment of charge mobility extraction in FETs. *Nat. Mater.* **2018**, *17*, 2−7.

(54) Deng, J.; Xu, Y.; Liu, L.; Feng, C.; Tang, J.; Gao, Y.; Wang, Y.; Yang, B.; Lu, P.; Yang, W.; Ma, Y. An ambipolar organic field-effect transistor based on an AIE-active single crystal with a high mobility level of 2.0 cm2/Vs. *Chem. Commun.* **2016**, *52*, 2370−2373.

(55) Lei, T.; Dou, J.; Cao, X.; Wang, J.; Pei, J. Electron-Deficient Poly(p-phenylene vinylene) Provides Electron Mobility over 1 cm2/Vs under Ambient Conditions. *J. Am. Chem. Soc.* **2013**, *135*, 12168−12171.

(56) Gierschner, J.; Park, S. Y. Luminescent distyrylbenzenes: tailoring molecular structure and crystalline morphology. *J. Mater. Chem. C* **2013**, *1*, 5818−5832.